


Reductive-co-precipitated cellulose immobilized zerovalent iron nanoparticles in ionic liquid/water for Cr(VI) adsorption

Archana Kumari Sharma · Rupesh S. Devan · Meenu Arora · Rabindra Kumar · Yuan-Ron Ma · J. Nagendra Babu 

Received: 10 March 2018 / Accepted: 5 July 2018 / Published online: 13 July 2018
© Springer Nature B.V. 2018

Abstract Microcrystalline cellulose immobilized zerovalent iron nanoparticles (CI-1-3) with different loading of 6, 12 and 24% w/w Fe⁰ were synthesized by NaBH₄ reduction under simultaneous co-precipitation of cellulose from ionic liquid ([BMIM]Cl)-water binary mixture. SEM, TEM, FTIR, VSM, XRD and XPS analysis were carried out to characterize the material. The electron microscopy studies revealed the immobilization of iron nanoparticle in the bulk and

surface of microcrystalline cellulose with a size range of 20–100 nm. CI-1-3 showed strong interaction between cellulose hydroxyl moiety and nZVI, immobilized on the polymer and saturation magnetization of 3 emu/g for CI-2. The materials were studied for Cr(VI) adsorption which revealed the q_{max} value of 28.57, 58.82 and 38.48 mg Cr(VI)/g of CI-1-3, respectively.

Electronic supplementary material The online version of this article (<https://doi.org/10.1007/s10570-018-1932-y>) contains supplementary material, which is available to authorized users.

A. K. Sharma · R. Kumar
Department of Environmental Science and Technology,
School of Environment and Earth Science, Central
University of Punjab, Bathinda, Punjab 151001, India

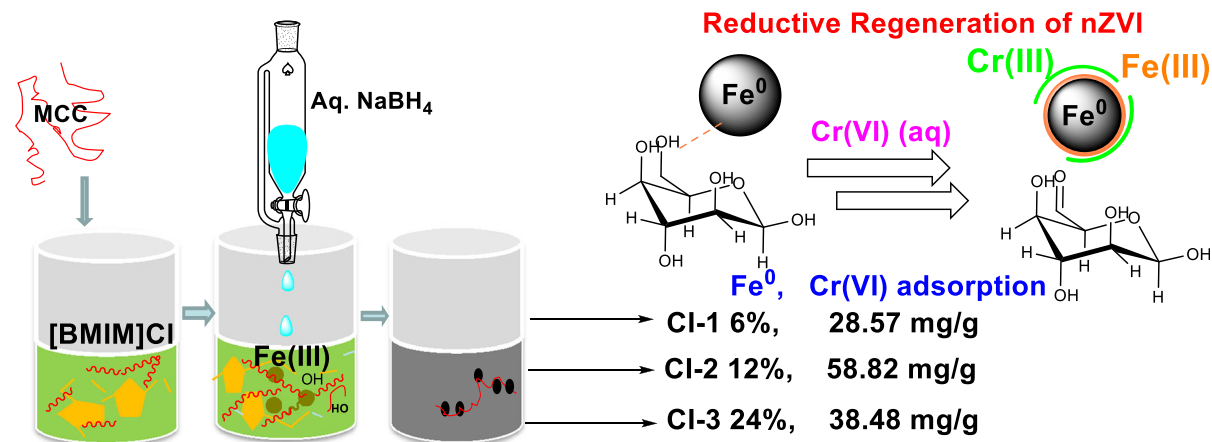
R. S. Devan
Discipline of Metallurgy Engineering and Materials
Science, Indian Institute of Technology Indore, Khandwa
Road, Simrol, Indore 453552, India

M. Arora
Department of Applied Chemistry, Maharaja Ranjit Singh
Punjab Technical University, Bathinda, Punjab, India

Y.-R. Ma
Department of Physics, National Dong Hwa University,
Hualien 97401, Taiwan

J. N. Babu (✉)
Department of Chemical Sciences, School of Basic and
Applied Science, Central University of Punjab, Bathinda,
Punjab 151001, India
e-mail: nagendra.rd@gmail.com

Graphical abstract



Keywords Microcrystalline cellulose · nZVI · Cr(VI) adsorption · Reductive regeneration · [BMIM]Cl · Ionic liquid

Introduction

Chromium, due to its wide usage in various industries such as electroplating, tanning, textile, and leather, is released into the environment in the form of treated industrial wastewater (Patterson and Passino 1987; Owlad et al. 2009). In the natural environment, chromium occurs in two oxidation states; Hexavalent chromium or Cr(VI) in the oxoanion form and Trivalent Chromium or Cr(III). Cr(VI) is highly mobile and toxic species when compared to Cr(III) which has low solubility and mobility (Koujalagi et al. 2013). Chromium is associated with various chronic and acute health effects in the human population including lung cancer, dermatitis, skin irritation and epigastric pain (NIEHS 2011; Sharma et al. 2012). As a consequence, the maximum permissible limit in drinking water is 0.01 mg/L for Cr(VI) and 0.10 mg/L for total Chromium (USEPA 2011), and in wastewater, its limit is 0.05 mg/L (USEPA 2013). Thus, Cr(VI) removal from drinking water is essential and carried out by various techniques namely, coagulation and sedimentation, electrocoagulation (Golder et al. 2007), precipitation (Guo et al. 2006), crystallization, Membrane filtration, Reverse osmosis (Hafez and El-Mariharawy 2004; Perez-González et al. 2012; Fu and

Wang 2011), ion exchange (Galan et al. 2005), adsorption (Jabeen et al. 2011), bioremediation (Xie et al. 2013), phytoremediation (Narayani and Vidya 2012; Miao and Yan 2013) etc. However, these methods are limited by costly technology, high operational and maintenance cost, skilled labour requirement: particularly in membrane filtration, and sludge disposal (Sharma et al. 2009; Hu et al. 2011). Of these methods, adsorption is the most appropriate, effective and versatile method for chromium removal.

Diverse form of organic, inorganic and natural bio-based materials were used for the removal of chromium, either as Cr(VI) and or Cr(III) by adsorption process such as, various biowaste (Parlayici and Pehlivan 2015; Kwak et al. 2015), chitosan fibres (Li et al. 2015), graphene (Jabeen et al. 2011), resin (Fu et al. 2013), Fly ash (Vaid et al. 2013), clay (Yadav et al. 2016; Fu et al. 2015) etc. Cellulose is a recalcitrant sustainable natural polymer, which has potential use as bio-adsorbent for various environment pollutants (Singha and Guleria 2014). However, cellulose has poor adsorption for Cr(VI) as such. Though, the modification of polymer surface with various functional moieties, like magnetic polyaniline nanocomposite cellulose (Qiu et al. 2015), Amidoximated Cellulose (Saliba et al. 2000), cellulose functionalized with quaternary ammonium moieties (Gurgel et al. 2009), cellulose anion exchanger with tertiary amine (Anirudhan et al. 2009), styrene grafted cellulose microsphere (Zhang et al. 2012), Oxidised polyaniline cellulose fibre composite (Liu et al. 2013) etc. have been used for Cr(VI) adsorption. These

derivatives show ion exchange or electrostatic interaction based adsorption for Cr(VI) oxoanion. However, these functional materials have the disadvantage of being costly, non-biodegradable and may release toxic secondary metabolites during the life cycle of the material.

Nanoscale zerovalent iron (nZVI) has a high surface area which leads to high reactivity and makes it an ideal sorbent for contaminant treatment (Crane and Scott 2012; Mukherjee et al. 2015; Stefaniuk et al. 2016). However, usage of nZVI in remediation is limited by either of the two phenomenon namely, agglomeration due to magnetic property of iron and surface passivation (Ponder et al. 2000). Surface passivation leads to the formation of iron oxide layer upon exposure to oxygen in the air, leading to loss of activity of the sorbent. Thus, various stabilizers and immobilizers have been studied for the stability of zerovalent iron nanoparticles (Trujillo-Reyes et al. 2014; Yadav et al. 2016). Polysaccharide-based stabilizers like starch (Alidokht et al. 2011), Chitosan (Horzum et al. 2013), Calcium alginates (Bezbaruah et al. 2009) and CMC (Singh et al. 2011) have been used in stabilizing and immobilizing iron nanoparticles. Most of these stabilizers are either water soluble or have enhanced microbial degradation susceptible to release and destabilize the nZVI. Recently, Datta et al. (2014) synthesized filter paper immobilized nZVI, that shows 64% Cr(VI) removal efficiency.

In an alternate approach cellulose has been used as a sustainable immobilizer has been utilized for various nanoparticles, including, TiO₂ (Duan et al. 2015), Cu, Ni (Kotelnikova et al. 2007), silver, gold, platinum (Cai et al. 2008) and nZVI (Raychoudhury et al. 2012). However, its usage and applications in nZVI is limited in its study. The poor solubility of cellulose in water and organic solvents restricts their broad application. However, the dissolution of cellulose in ionic liquid (Swatloski et al. 2002; Zhu et al. 2006) has broadened its usage in various application including, fuel cell (Sajana et al. 2014), sensing (Hines et al. 2008), bioethanol (KleinKlein-Marcuschamer et al. 2011; Fitz-Patrick et al. 2010), environmental remediation (Liu et al. 2012), nanoelectronic devices (Seid et al. 2012). However, limited studies have been carried out in the synthesis of cellulose immobilized nanomaterials in the ionic liquid. Gelesky et al. (2009) synthesized Pt and Rh nanoparticle immobilized on cellulose acetate film using ionic liquid 1-n-Butyl-3-

methylimidazolium bis(trifluoromethanesulfonyl)imide (BMI.NTf₂). Similarly, magnetic cellulose-chitosan hydrogel has been synthesized using ionic liquid by Liu et al. (2012), which showed high removal efficiency for Pb²⁺, Fe²⁺ and Cu²⁺ ions.

Recently, we reported unusual adsorption of Cr(VI) up to 562.8 mg/g of nZVI by cellulose immobilized nZVI material synthesized in an aqueous medium (Sharma et al. 2015). Thus in continuation, the present study investigates the Cr(VI) adsorption characteristics of nZVI loaded cellulose (CI-1-3) synthesized by borohydride reduction with simultaneous co-precipitation of polymer from the ionic liquid.

Materials and methods

Microcrystalline cellulose Avicel PH-101[®] obtained from Sigma Aldrich (St. Louis, USA) and all other chemicals used in the study were of analytical purity. Deionized water was used for the preparation of chemical and reagent. Total chromium and hexavalent chromium in adsorption studies were determined using diphenylcarbazide method (APHA 2005). Iron estimation of CI-1-3 was carried out by phenanthroline method, upon HNO₃/H₂SO₄ digestion of the sample (Harvey Jr. et al. 1955).

Physical characterization of cellulose immobilized nZVI (CI-1-3)

Fourier Transformed Infrared (FTIR) spectra of Microcrystalline Cellulose (MCC), dried CI-1-3 and chromium adsorbed CI-1-3 were recorded on an FTIR (BRUKER TENSOR 27). Transmission Electron Microscope (TEM) analysis was obtained on Technai200 kV TEM. Morphological characterization was carried out by Scanning Electron Microscope (FE-SEM) using Carl Zeiss, Merlin Compact 6073. CI samples were coated with gold before the SEM analysis. Electron Dispersive X-rays spectroscopy (EDX) analysis performed on Oxford maxN. CI samples were coated with gold before the SEM analysis. Magnetization studies were performed on a Vibrating Sample Magnetometer (VSM) (Lakeshore Model: 7404, USA) with the maximum magnetizing field of 1.2 Tesla in an inert vacuum atmosphere. Thermogravimetric analysis (TGA) was carried out at a heating rate of 10 °C/min up to 500 °C using a

Shimadzu TG-60H TG analyzer under N₂ environment. Powdered X-ray diffraction (XRD) analysis was carried with CuK α radiation ($k_p = 1.54056 \text{ \AA}$) and X-ray photoelectron spectroscopy (XPS) analysis (VG Multilab 2000-Thermo Scientific, UK, K-Alpha) with a multi-channel detector, which can endure high photonic energies from 0.1 to 3 keV). CHN elemental analysis for chromium adsorbed CI-2 was carried out using Thermo-Finngan elemental analyser. Chromium solution upon adsorption analysed by U-Vis Spectrophotometer at a wavelength of 540 nm.

Adsorption experiments

The adsorption experiments for Cr(VI) using CI-1-3 was carried out in triplicate. For this, a stock solution (1 mM) was prepared in deionized water by dissolving 294 mg of K₂Cr₂O₇ in 1000 mL of deionized water. Standard Cr(VI) solution 1–10 mg/L, were prepared for adsorption study. To a 100 mL of Cr(VI) solution (1–10 mg/L), 10 mg of CI-1-3 were added and incubated at 25 \pm 2 $^{\circ}$ C and 200 rpm for 24 h. The samples were filtered using Whatman filter paper 1 and analysed by the dipheylcarbazide method at a wavelength of 540 nm using U-Vis spectrophotometer. The optimization study was carried out for parameters like pH, dose and initial concentration. pH of the Cr(VI) solution was maintained at 3, 5, 7, 8 and 10 using 1 N HCl and/or NaOH solution at Cr(VI) concentration of 5 mg/L with a dose of 100 mg/L of CI-1-3. The dose experiment was carried out using 3 mg/L of chromium solution at the optimum of pH 3 with varying amount of CI-1-3 (50, 100, 200 and 400 mg/L).

Kinetic study of Cr(VI) by CI-1-3

Adsorption of Cr(VI) using CI-1-3 was analysed by contact time study for optimization of equilibration time and kinetics of adsorption. To a 100 ml solution of 20 mg/L Cr(VI) was added 10 mg of CI-1-3 and incubated at 25 \pm 2 $^{\circ}$ C, 200 rpm for 24 h. A small aliquot was drawn and analyzed at various time intervals, i.e. 30, 60, 120, 180, 240, 360, 480, 600, 840 and 1440 min and diluted accordingly for analysis. The concentration of Cr(VI) adsorbed was plotted as a function of time. The data was studied for its pseudo-first order and pseudo-second-order kinetic behaviour.

Interference study for Cr(VI) adsorption by CI-2

To a 50 ml of 6 mg/L Cr(VI) solution was added the desired volume of stock solution of various salts. The solution was adjusted to pH 3 with makeup to give a 3 mg/L Cr(VI) with various salts were maintained at 10, and 100 mg/L and CI-2 amount of 200 mg/L were added and incubated at 25 \pm 2 $^{\circ}$ C, 200 rpm for 24 h.

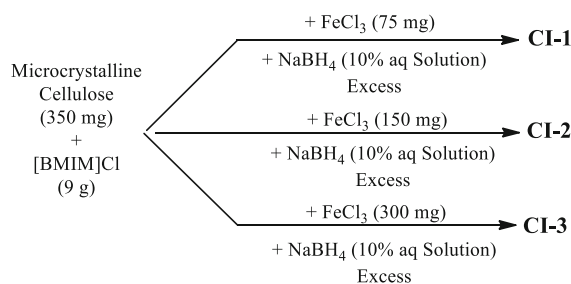
Regeneration study of chromium by CI-2

The chromium concentration of 1000 mg/L with 1 g/L of CI-2 was used for the regeneration study at pH 3 for 24 h at 25 \pm 2 $^{\circ}$ C. After 24 h of reaction, the chromium solution was decanted from the CI-2 material. Without any further treatment, the CI-2 was used for adsorption of the chromium from a fresh Cr(VI) solution. The filtrate was collected separately upon adsorption. The above said method was repeated 4 times with the residue containing CI-2, with fresh Cr(VI) solution. The filtrate collected were analyzed for Cr(VI) using phenanthroline method.

Result and discussion

Synthesis and characterization of CI-1-3

The ionic liquid [BMIM]Cl was prepared using the method reported by Crowhurst et al. 2003. The CI-1-3 was synthesized by dissolution of cellulose in [BMIM]Cl, a desired amount of FeCl₃ followed by dropwise addition of aqueous NaBH₄ to furnished CI-1, CI-2 and CI-3 (6, 12 and 24% w/w) with instantaneous reduction of iron with simultaneous precipitation of cellulose and nZVI (Scheme 1).



Scheme 1 Synthesis of microcrystalline cellulose immobilized nZVI (CI-1-3)

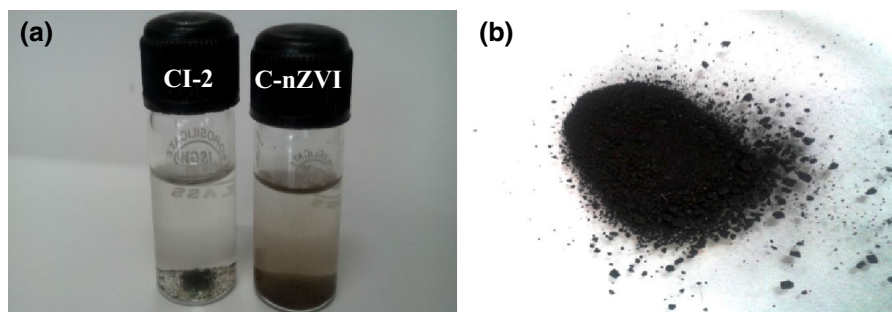


Fig. 1 **a** Stability of CI-2 and C-nZVI in tap water (pH = 8.15 TDS = 970 mg/L) upon standing for 48 h and **b** CI-2 after 90 days under ambient conditions

The iron content of the CI-1-3 were analyzed using phenanthroline method (Harvey Jr. et al. 1955). The analysis revealed iron loading in CI-1-3 to be 6.4, 12.02 and 24%, respectively. The result indicated the presence of iron in CI composite is proportional to the amount of FeCl_3 used for synthesis.

Stability study of CI-1-3 and microcrystalline cellulose immobilized nZVI synthesized in water (C-nZVI)

CI-2 and C-nZVI (Sharma et al. 2015), respectively with 12% w/w iron loading on cellulose were studied for their stability upon a stay in groundwater sample (Fig. 1a). CI-2 was stable for 48 h, whereas C-nZVI turned brown in 10 h, i.e. an oxide of iron was formed in the presence of water. Apart from this CI-2 showed better air stability with more than a year shelf life (Fig. 1b), whereas C-nZVI was found to lose its activity within 30 days under ambient conditions. This stability of CI-2 over C-nZVI is accounted for the stabilization of iron nanoparticle by its immobilization in cellulose bulk.

Characterization of microcrystalline cellulose immobilized nZVI (CI-1-3)

SEM analyses were carried out for the morphological characterization of cellulose immobilized zerovalent iron nanoparticle (CI-1-3) (Fig. 2a–c). SEM images of the CI-1-3 showed that the iron nanoparticles were immobilized on cellulose polymer. The size of the nZVI particles lie in the range of 20–100 nm and were spherical in shape. SEM image of CI-1 (Fig. 2a) showed that fewer nZVI particles were embedded on the cellulose surface with limited surface occupancy

of nZVI on the polymer, leaving large surface area of polymer unoccupied due to the lower amount of iron. However, there is an increase in the density of nZVI on the surface of cellulose with lesser surface remaining unoccupied in case of CI-2. The nZVI were found to be agglomerated on the surface of cellulose due to the magnetic properties of Fe^0 (Ponder et al. 2000) (Fig. 2b). Upon increasing the iron content to 24% w/w in CI-3, there is a significant change in the morphology and arrangement of nZVI on the cellulose surface. The iron particles were extremely agglomerated to form a plate-like structure on the surface of cellulose. Due to the high concentration of iron, the particles synthesized were submicron-sized particles, and no space was left unoccupied on the cellulose surface. The images suggest that water is a precipitating solvent for cellulose and addition of aqueous NaBH_4 solution to the cellulose-Fe(II) solution in the ionic liquid lead to a reduction of iron and precipitation of cellulose simultaneously, thus leading to variedly embedded CI-1-3.

TEM analysis of CI-1-3 was carried out for the characterization of iron immobilization on the surface and core of cellulose. TEM images of CI-1-3 showed an embedding of nZVI on the cellulose framework (Fig. 2d–f), with increasing concentration of iron-loaded on to cellulose. The image of CI-2 shows chain like agglomeration of nZVI embedded in cellulose. This indicates the reduction of iron being faster than MCC precipitation. In comparison to CI-2, CI-3 showed increased deposition of iron on the surface of cellulose with fewer iron particles occupying the core of cellulose. This suggests that upon increasing the loading of iron, the precipitation of cellulose was faster than the reduction of iron. As the reduction occurs in two steps, whereby reduction of Fe(III) to

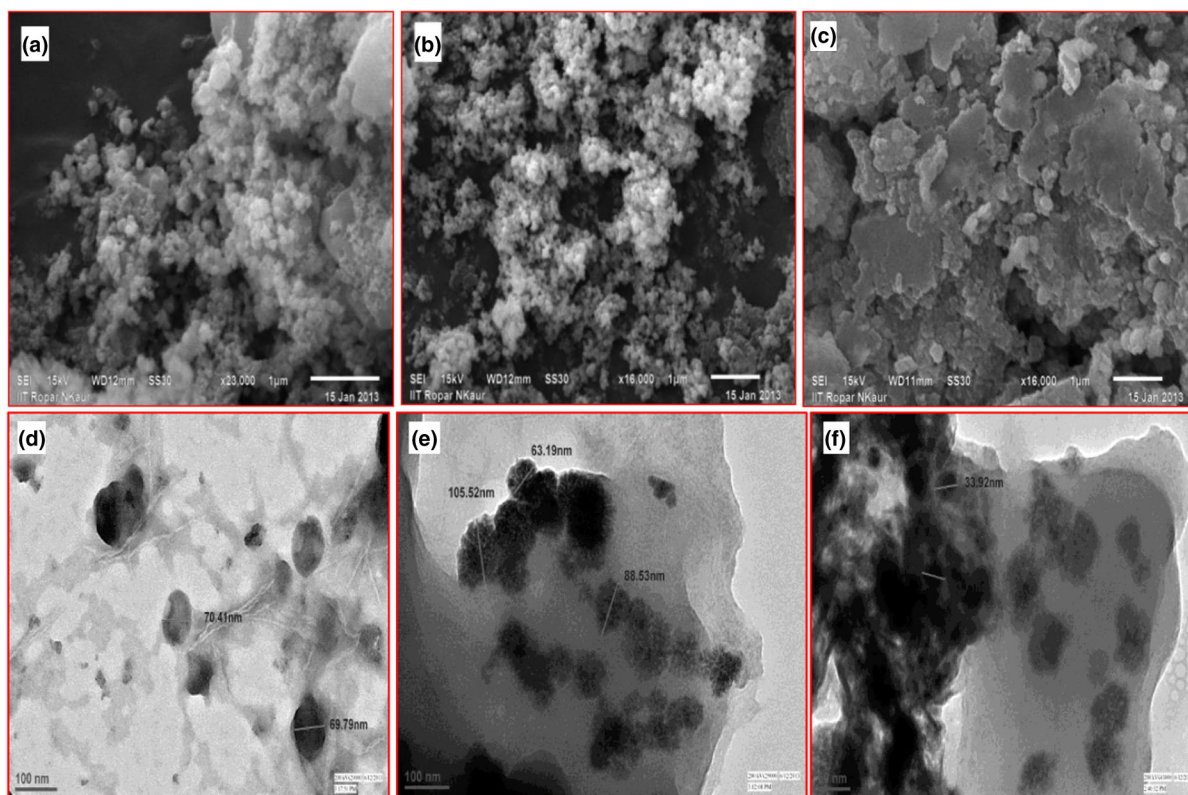


Fig. 2 SEM images of **a** CI-1, **b** CI-2 and **c** CI-3; TEM images of **d** CI-1, **e** CI-2 and **f** CI-3

Fe(II) is fast and spontaneous whereas further reduction of Fe(0) is slow. Thus, upon increasing the concentration of iron in CI-3, complete reduction of Fe(III) to Fe(0) does not take place to precipitate iron before the precipitation of cellulose, leading to superficial immobilization of iron onto cellulose.

FTIR studies were carried out for establishing the surface interaction between nZVI and Microcrystalline cellulose in CI-1-3 as given in Fig. 3. MCC was characterized by the presence of absorption bands at 3424 cm^{-1} which corresponds to hydrogen bonded hydroxyl groups (Lu and Hsieh 2010). Upon immobilization of nZVI on MCC, a shift in the absorption band with narrowing, centered at 3357, 3360 and 3400 cm^{-1} , respectively, for CI-1, 2 and 3 were observed. This narrowing of the absorption band in this region shows the interaction of hydroxyl moieties of cellulose with nZVI in these materials. This interaction could be elaborated as of the kind Fe.....HO (Jones et al. 1998; He et al. 2007). The absorption band at 946 and 825 cm^{-1} in case of CI-1-2 is accounted to the shift in the C-O_{str} due to the strong

hydrogen bonded interaction between MCC and nZVI (Xiao et al. 2009). However, the adsorption band at 946 cm^{-1} is absent in case of CI-3 because of the high amount of iron create inter-particle interaction between iron thereby aggregating nZVI and compromising interaction between nZVI and MCC.

The FTIR spectrum of chromium adsorbed CI-2, showed a band broadening in the region of $3000\text{--}3400\text{ cm}^{-1}$ corresponding to the weakening of hydrogen bonding between the nZVI and MCC. A band broadening at 1200 cm^{-1} corresponds to C-O_{str} stretching. This suggests that due to change in the surface morphology of the iron nanoparticle, there is a significant change in the binding of the nZVI to the surface of the MCC (Sharma et al. 2015). The two characteristic absorption bands of C-O_{str} at 946 and 825 cm^{-1} disappeared in case of CI-2 upon chromium adsorption. Further, a new absorption band was observed at 1740 cm^{-1} in case of chromium adsorbed CI-2, which is accounted to the carbonyl moiety. This carbonyl functional group suggests the formation of cellulose dialdehyde (Kim et al. 2004; Sharma et al.

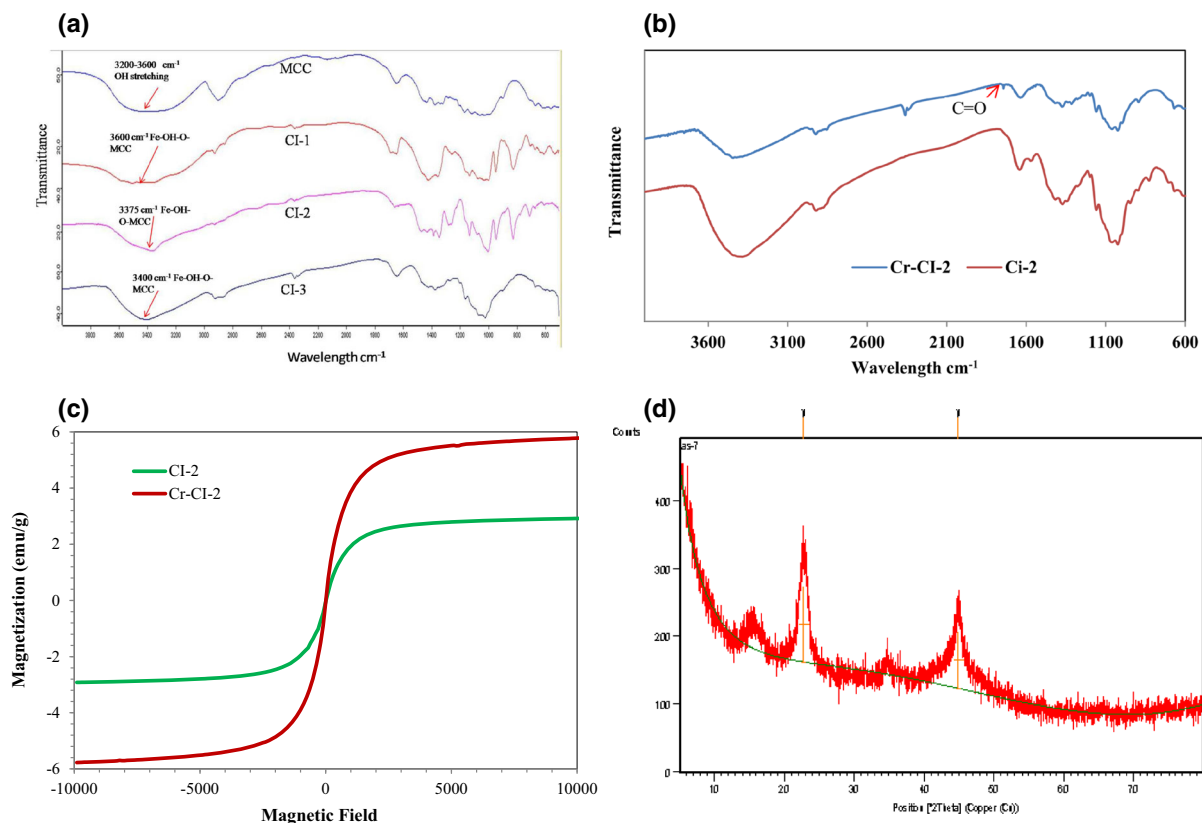


Fig. 3 FTIR spectra of **a** MCC and CI-1–3, **b** CI-2 and Cr(VI) adsorbed CI-2, **c** magnetization curve of CI-2 and CI-2 after adsorption of Cr(VI), **d** XRD pattern of CI-2

2015). For the investigation of dialdehyde formation, CHN analysis of Cr adsorbed CI-2 was carried out upon oxime derivatization. The presence of 0.47% of nitrogen confirms the formation of dialdehyde upon adsorption of Cr by CI-2 (Fig. S7). Thus, it confirms the in situ reductive regeneration of nZVI in case of CI-2, similar to that reported for cellulose immobilized nZVI synthesized in a water medium (Sharma et al. 2015).

The magnetic property of CI-2 and its chromium adsorbed residue was verified by VSM studies as depicted in Fig. 3c. The saturation magnetization moment of Cr adsorbed CI-2 (6 emu/g) is higher than CI-2 (3 emu/g), which is less than that of nZVI (Jabeen et al. 2011). The material CI-2 shows superparamagnetic property, that has no corecivity and residual magnetization (Dalla Vecchia et al. 2009). This could be accounted to the immobilization and encapsulation of nZVI by cellulose in the synthesis process, which upon Cr(VI) adsorption is regenerated

by in situ reduction by cellulose which weakens the binding between the exposed cellulose–dialdehyde and nZVI leading to the characteristic increase in the magnetization.

The XRD pattern of CI-2 showed a characteristic peak of metallic iron (Fe⁰) at 2θ = 44.8° (index 110) on cellulose surface (Fig. 3d). Further, the reflections at 2θ = 22.7 and 35.0° suggest the existence of cellulose in cellulose-I crystalline form (Yu et al. 2013; de Moraes Teixeira et al. 2010).

Thermogravimetric analysis (TGA) and differential thermogravimetric analysis

The thermal stability of CI-2 and CI-3 were studied and compared with Microcrystalline cellulose (MCC) by TGA and DTA analysis (Fig. 4a, b). MCC underwent thermal degradation in the temperature range of 300–350 °C (up to 90% weight loss) while CI-2 degraded in two stages in the temperature range of

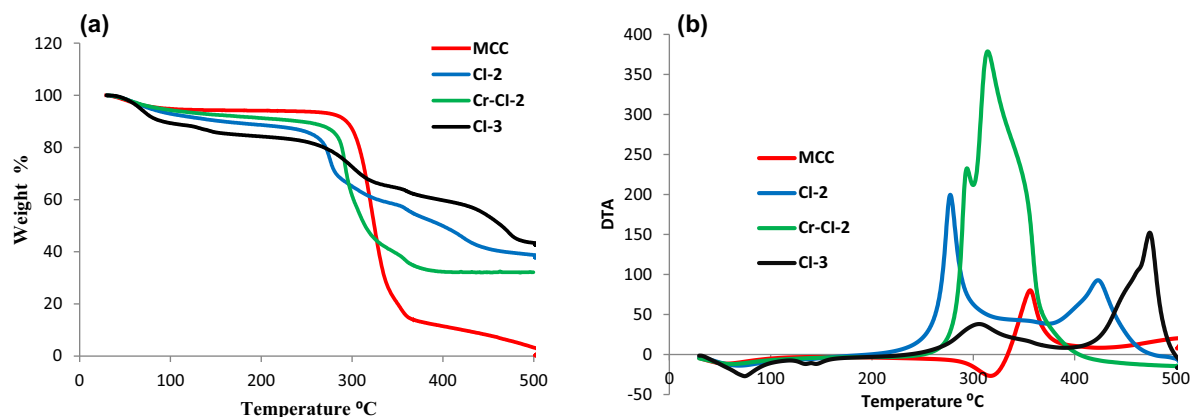


Fig. 4 **a** TGA and **b** DTA analysis of MCC, CI-2 and CI-3 and Cr adsorbed CI-2

270–280 °C and 300–345 °C. Similarly, CI-3 degraded in the temperature range of 290–370 °C in the first stage and 390–480 °C in the second stage. The degradation of CI-2–3 at lower temperature establishes its poor stability in comparison to MCC. The lower weight loss in case of CI-2 and 3 with respect to MCC at temperature > 350 °C, is due to the oxidation of Fe⁰ to Fe₃O₄ (Yadav et al. 2016; Yu et al. 2013). The difference in the degradation temperature of CI-2 and CI-3 is accounted to the presence of high amount of iron in CI-3. This high amount of iron creates agglomeration in CI-3, due to which outer iron surface is oxidized and prevents oxidation of iron core. A part of CI-2 and CI-3 degraded at a higher temperature, which is accounted to the oxidation of charred carbon residues on the oxidized iron. The residue left in case of CI-2 and CI-3 was 38 and 42%, respectively. The higher ash content in case of CI-3 is accounted to the higher loading of iron. However, the weight loss in case of CI-2 and CI-3 is lower than that of MCC, as char formation occur in the presence of iron. The Cr adsorbed CI-2 showed degradation similar to MCC. The Cr adsorbed CI-2 showed thermal degradation of cellulose in a narrow temperature range of 280–350 °C, which is significantly similar to the TG pattern of cellulose dialdehyde (Kim and Kuga 2001). There is no significant change observed up to 500 °C, which indicates that iron is in completely oxidized form. But the residual content was significantly higher as compared to CI-2 and MCC, which accounts for the oxidation of iron and adsorption of Cr(VI).

The DTA curve of MCC shows heat loss in the temperature range from 100 to 330 °C, further heat gain was observed at a temperature of 358 °C (Fig. 4b). Upon loading of iron on cellulose, incase of CI-2, heat gain was observed at a temperature of 275 and 405 °C. At a temperature interval of 450–500 °C, drastic heat loss was observed in case of CI-2, whereas, CI-3 showed heat loss at a temperature of 300 °C, further high heat loss was observed at 475 °C. The lower heat loss in CI-2 is due to the presence of lower amount of iron for oxidation as compared to CI-3. The agglomeration of iron on the cellulose surface prevents the cellulose oxidation. Upon adsorption of chromium on CI-2, a significant amount of heat loss was observed at a temperature of 315 °C, and in the temperature range of 475–500 °C. This suggests the formation of chromium-iron complex.

X-ray photoelectron spectroscopy (XPS) analysis

The XPS analysis of CI-2 and CI-3 in Fig. 5 shows depth profile of Fe⁰, Fe(II or III), O, C and Cr of the particles with 12 and 24% w/w of loading of iron without and with adsorbed chromium (Fig. 5a–d). For precise determination of the features of the peaks in each spectrum, all spectra are deconvoluted via Voigt curve fitting within the Shirley background. The photoelectron peak corresponding to the binding energy of Fe(2P_{3/2}) and Fe(2P_{1/2}) observed at 710.21 and 723.37 eV, respectively (Wen et al. 2014; Li and Zhang 2007), ascertains the existence of iron in the

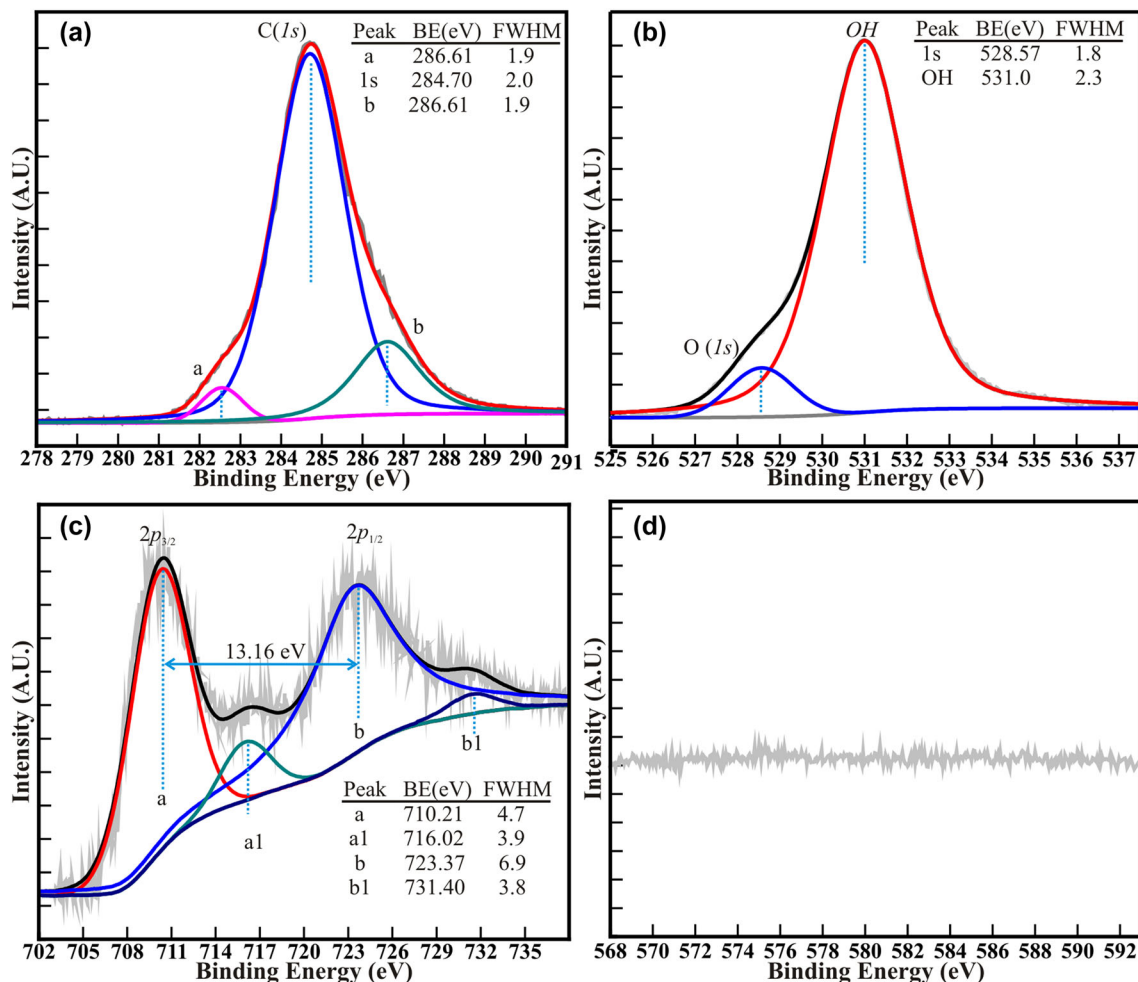


Fig. 5 High-resolution XPS spectra for the core level of **a** C, **b** O, **c** Fe and **d** Cr for the sample CI-2

zero-valence state (Fe^0). Pilot peaks at 716.02 and 731.40 eV correspond to the binding energy of Fe_2O_3 that reveals the nZVI surface was covered with a small layer of iron oxide. The binding energy peak, observed at 531.0 and 528.57 eV corresponds to the binding energy of OH group of cellulose and Fe–O layer of iron on the surface, respectively (Manning et al. 2007; Devan et al. 2011, 2016, 2017; Moulder 1992). The double peak features of C(1s) core level located at a binding energy of 284.7 and 286.6 eV confirm the presence of carbon on cellulose as C–C and C–O–C bond, respectively (Matuana et al. 2001). Moreover, the absence of Cr has been confirmed in CI-2 sample (Fig. 5d).

Upon adsorption of Cr onto CI-2 as well as CI-3, the photoelectron peak of Fe(2p) core levels showed no shift in the binding energy of Fe($2P_{3/2}$) and Fe($2P_{1/2}$),

indicates the presence of Fe^0 (Figs. 6a, 7a). Figure 6b depicts the peaks corresponding to core levels of Cr($2P_{3/2}$) and Cr($2P_{1/2}$) at a binding energy of 575.86 (Halada and Clayton 1991) and 585.49 eV (Li et al. 2008). However, the comparison of CI-2 with chromium adsorbed CI-2, showed an increase in the intensity of the peak located at a binding energy of 715.49 and 731.98 eV, respectively, corresponding to Fe($2P_{1/2}$) and Fe($2P_{3/2}$) of Fe(III/II), (Fig. 6a). This suggests the increase in the Fe(II/III) concentration in Cr adsorbed CI-2.

A comparison of CI-2 and Cr adsorbed CI-2 showed an increase in the intensity of binding energies corresponding to Cr, confirmed the presence of adsorbed chromium on the surface of the material (Figs. 5d, 6b). The peaks observed at a binding energy of 575.86 and 585.49 eV suggest the presence of

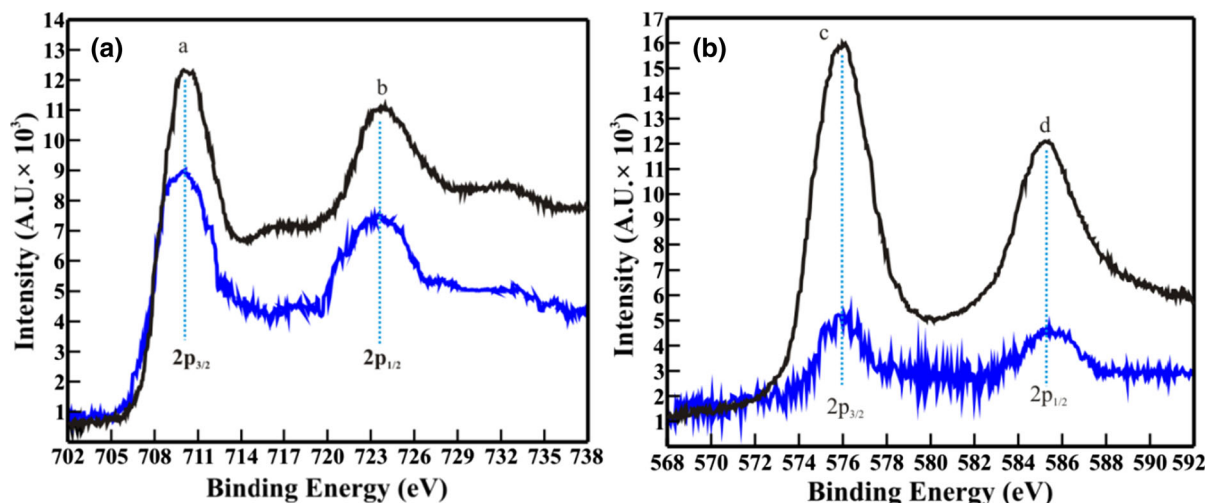


Fig. 6 High-resolution XPS spectra of chromium adsorbed CI-2 (blue) and CI-3 (black) depicting the binding energy spectrum of **a** iron, **b** chromium. (Color figure online)

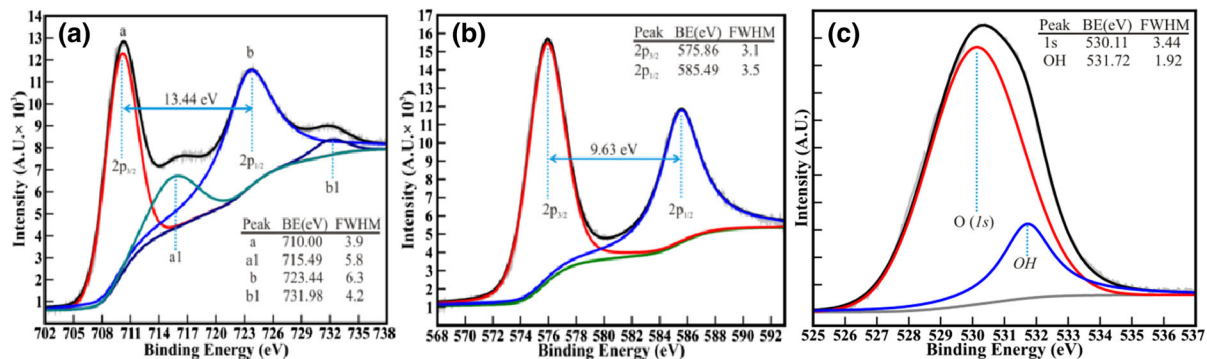


Fig. 7 High-resolution XPS spectra of chromium adsorbed CI-3 depicting the binding energy spectrum of **a** iron, **b** chromium and **c** oxygen

chromium in the Cr(III) state. Thus, during adsorption of chromium onto CI-2, Fe⁰ is oxidized to Fe(II or III), reducing Cr(VI) in the solution to Cr(III) immobilized on surface of nZVI immobilized on cellulose. This, in turn, leads to the formation of a precipitate of Fe(II or III)–Cr(III) oxide. Similar variation was observed for Cr(III) in case of chromium adsorbed CI-3 (Fig. 7b). Further, Cr adsorbed CI-3 showed a satellite peak at 531.72 eV and an intense peak at 530.11 eV, is attributed to OH and oxides, respectively in the material (Fig. 7c) (Devan et al. 2010; Moulder 1992). A comparison of the peak intensities of OH and oxide in CI-2 and chromium adsorbed CI-3 showed an increase in the intensity of the oxide peak and decrease in the intensity of hydroxyl peak. The increase in oxide indicates the oxidation of zero-valent

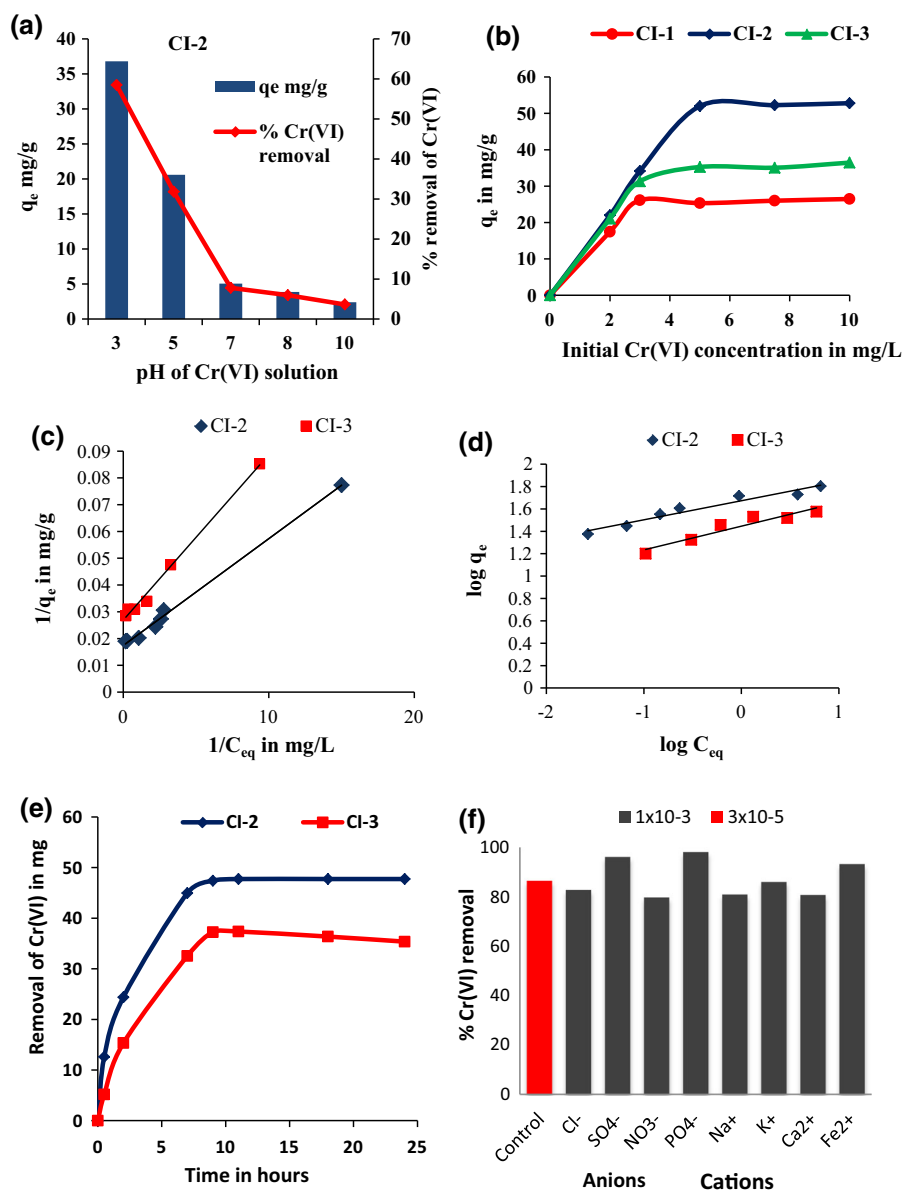
iron as well as oxidation of cellulose. However, lowering of the intensity of binding energy peak corresponding to OH at 531.72 eV confirms the oxidation of cellulose or presence of hydroxyl groups in CI-2 (Devan et al. 2009).

Adsorption studies

Effect of pH on Cr(VI) adsorption

In adsorption process, pH plays a vital role, particularly for ionic species like Cr(VI). Thus, CI-2 was studied for the effect of pH on the Cr(VI) removal by reductive-adsorption in the pH range 3–10. The result of the adsorption, in terms of the Cr(VI) removal efficiency is as given in Fig. 8. The CI-2 was found to

Fig. 8 Effect of a pH by Cr(VI) = 5 mg/L, CI-2 = 100 mg/L, b initial Cr(VI) concentration = 1–10 mg/L, CI-2 = 100 mg/L, pH-3, c Langmuir and d Freundlich adsorption isotherm for CI-2-3 for adsorption of Cr(VI), e contact time using Cr(VI) = 20 mg/L, CI-2-3 = 100 mg/L, f effect of Various Anions and Cations in the concentration of 1×10^{-3} M on Cr(VI) (3 mg/L) adsorption by 100 mg/L of CI-2



remove Cr(VI) with an efficiency of 36.8, mg/g at pH 3 which is reduced to 2.4 mg/g at pH 10 (Fig. 8a). Thus, the removal efficiency was observed to be maximum under acidic conditions. This could be explained by, the surface protonation of nZVI leading to positively charged surface favoring electrostatic interaction with Cr(VI) oxoanion (Jabeen et al. 2011). Further, the protonation of chromate ion reduces the anion-nZVI electrostatic repulsion thus facilitating adsorption at low pH (Gheju 2011; Li et al. 2008). But, as the pH increases, the availability of protons is significantly

decreased reducing the electrostatic attraction between Cr(VI) and nZVI. It was further observed that CI-2 suspension is primarily black in color/appearance. It undergoes a significant change in the color upon treatment with Cr(VI) solution. This change of color signifies the oxidation of Fe⁰ to Fe(III) and formation of Cr(III)–Fe(III) hydroxide precipitates (Powell et al. 1995).

Effect of dosage of CI-2 on Cr(VI) adsorption

The efficiency for Cr(VI) removal increased from 34.73 to 83.85%, upon increasing the CI-2 dosage from 50 to 100 mg/L as depicted in Fig. S3. However, when the dosage of CI-2 was further increased to 200 and 400 mg/L, there was a significant increase in the removal efficiency of Cr(VI) which reaches a saturation level at 91.92 and 93.68%, respectively. Thus, the optimum dose for the adsorption experiment was fixed at 100 mg/L Cr(VI) in an aqueous solution maintained at pH 3.

Effect of Cr(VI) concentration on adsorption by CI-1, 2 and 3

Cr(VI) adsorption was studied for CI-1-3 as shown in Fig. 8b. 100 mL of 1 to 10 mg/L range of chromium concentration were treated with 100 mg/L CI-1-3 at pH 3. The result showed CI-2 had higher removal efficiency than CI-3 followed by CI-1 (Table 1).

Adsorption Isotherm studies

Langmuir and Freundlich adsorption isotherm were used to determine the adsorption equilibrium between the nZVI and Cr(VI). The adsorption behavior of CI-1-3 was carried out for Cr(VI) as given in Fig. 8c, d, which is fitted to a linear model of Langmuir and Freundlich isotherm using equation 1 and 2. The Langmuir and Freundlich adsorption isotherm was best fitted for Cr(VI) adsorption using CI-1-3. The isotherm of CI-2 and CI-3 showed a linear fit for the plot between $1/C_{eq}$ and $1/q_e$ as shown in Fig. 8c. The isotherm plot for CI-3 is shown in supplementary Fig. S2. The maximum adsorption (q_{max}) was found to be 28.57, 58.82 and 38.48 mg of Cr(VI)/g for CI-1, 2 and 3, respectively (Table 2). The normalized adsorption value (q_n) was calculated according to the

Table 2 Kinetics constant for adsorption of chromium on CI-2 and CI-3

CI-2 20 mg/L	CI-3 20 mg/L
<i>Pseudo-second-order</i>	
$K_p = 9.2 \times 10^2 \text{ g}^{-1} \text{ mg}^{-1} \text{ h}$	$K_p = 2 \times 10^2 \text{ g}^{-1} \text{ mg}^{-1} \text{ h}$
$R^2 = 0.987$	$R^2 = 0.987$

percentage of iron loading on to CI-1-3 using equation given below:

$$\text{Normalized adsorption } q_n = \frac{q_e}{\%Fe} \times 100$$

The normalized value for Cr(VI) is 476, 490 and 160 mg of Cr(VI)/g of nZVI for CI-1, 2 and 3, respectively. CI-2 showed higher normalized removal efficiency for Cr(VI) than CI-3, which is the optimum loading for the Cr(VI) adsorption. The higher removal efficiency of CI-2 is comparable to that of CI-1, which accounts for the retain surface dispersion and nZVI activity on the cellulose surface. However, in case of CI-3, the iron particles are aggregated on the surface of cellulose, thus lowering the interaction between nZVI and cellulose surface leading to lower adsorption efficiency.

Kinetics equilibrium study

The removal efficiency for Cr(VI) (20 mg/L) increased from 4.18 to 47.74% upon increasing the contact time from 30 min to 24 h as depicted in Fig. 8e. The optimal removal efficiency was achieved at 11 h. In comparison to the literature on nZVI, the CI-3 showed slower Cr(VI) removal kinetics, which could be accounted to the lesser exposure of polymer embedded nZVI particles for adsorption of the Cr(VI).

The kinetic data showed best fit with the pseudo-second-order kinetic model for upon adsorption of

Table 1 Comparison of Langmuir and Freundlich constant for CI-1-3

Sample code	Langmuir				Freundlich			Normalized adsorption value of CI in mg/g
	q_e (mg/g)	K_L	R_L	R^2	Log K	1/n	R^2	
CI-1	28.57	0.008	0.813	0.970	0.226	0.772	0.738	476
CI-2	58.82	0.004	0.809	0.995	0.170	0.597	0.942	490
CI-3	38.48	0.006	0.812	0.994	0.212	0.692	0.900	160

Cr(VI) ions using CI-2 and CI-3 (Fig. S4 and S5). The result further showed that the rate constant was 9.2×10^2 and $2 \times 10^2 \text{ g}^{-1} \text{ mg}^{-1} \text{ h}$ for CI-2 and CI-3, respectively. The results indicate the better rate of adsorption by CI-2 to the extent of 4000 times better than that of CI-3. This may be accounted for the formation of micron-sized aggregates of iron.

Study of interference of ions on chromium adsorption

As CI-2 was prepared to immobilize and stabilize nZVI for groundwater and wastewater application. The CI-2 showed substantial adsorption for Cr(VI) from aqueous solution. Thus, it is essential to study the potential interference from major anions and cations present in the groundwater system. Thus, for the study of interference various anions using sodium salts of Cl^- , PO_4^{3-} , SO_4^{2-} and NO_3^- and cations using chloride salts namely Fe^{2+} , Ca^{2+} , K^+ and Na^+ in the concentration of 1×10^{-4} , 1×10^{-3} and $1 \times 10^{-2} \text{ M}$ were used. The CI-2 dose of 200 mg/L were added to 3 mg/L of Cr(VI) solution containing 1×10^{-4} , 1×10^{-3} and $1 \times 10^{-2} \text{ M}$ solution of various anions and cation maintained at pH 3. There was no significant change observed in the adsorption of Cr(VI) in the presence of anions; chloride and nitrate, and in presence cations, of Na^+ , K^+ , and Ca^{2+} as shown in Fig. S6. The effect of various anions and cations ($1 \times 10^{-3} \text{ M}$) is shown in Fig. 8f. However, anions PO_4^{3-} , SO_4^{2-} and cation Fe^{2+} , ions in the concentration of $1 \times 10^{-3} \text{ M}$ showed strong synergistic effect leading to the efficient removal of Cr(VI) ions. This synergistic effect could be accounted to the precipitation of the reduced chromium as $\text{Cr}(\text{SO}_4)_3$ and CrPO_4 , thus reducing the surface passivation of cellulose immobilized nZVI. The synergistic effect of Fe^{2+} ions could be accounted to the increased Cr(VI) reduction, subsequently followed by the adsorption in case of CI-2 (Kim et al. 2012).

Regeneration study of Cr(VI) by CI-2

In the regeneration study of Cr(VI) adsorption using CI-2, four successive generation of usage of CI-2 for Cr(VI) reductive adsorption was found to be significant. The result showed 44.63% of Cr(VI) removal in the first cycle which was reduced to 22.6% in the second cycle. The adsorption efficiency was lost

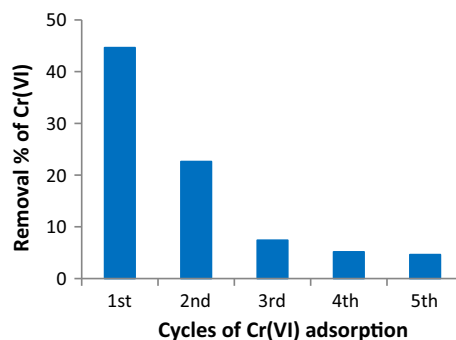


Fig. 9 Regeneration study of cellulose immobilized nZVI composite CI-2 (1 g/L) for Cr(VI) (pH = 3, 1 L, 1 g/L, 24 h, 200 rpm) adsorption

significantly at third and subsequent cycles in the range 6.56–4.64% (Fig. 9).

Discussion

The significantly high adsorption efficiency of chromium by CI-1-3 is due to reductive regeneration of zerovalent iron as cellulose is oxidized to form dialdehyde which regenerate zerovalent iron. Upon comparison of the loading characteristics of the CI-1-3, an increase in Cr(VI) adsorption up to twofold upon increasing the iron loading on cellulose from 6 to 12% is observed. Further increase in iron loading to 24%, a significant drop in the adsorption capacity of material was observed in case of CI-3. This trend in Cr(VI) adsorption upon loading was compared for normalized adsorption, similar normalized adsorption was observed in case of CI-1 and CI-2, approximately with a threefold higher Cr(VI) adsorption in comparison with CI-3. This characteristic adsorption behaviour of CI-1-3 could be attributed to the particle size of nZVI as well as the maximum coverage on the surface of cellulose. The particle sizes of ZVI immobilized on cellulose were characterized by nanodimension in case of CI-1 and-2, whereas in case of CI-3 the ZVI were plate shaped with size ranging in submicron. Similar results reported by Uzum et al. (2009) and Yadav et al. (2016), where the immobilized nZVI showed an optimum adsorption up to a certain loading onto the immobilizer, were observed with various other adsorbates like Cu(II), Co(II), As(V) As(III) etc. Similar loading characteristics has been studied by Uzum et al. (2009) on Cu(II) and

Table 3 Comparative evaluation of adsorption capacity of chromium by various adsorbent

S.N.	Adsorbent	Iron loading %w/w	Adsorption (mg/g)	Normalized adsorption efficiency (mg/g)	References
1.	Chitosan-nZVI	77.6	148.06	190	Geng et al. (2009)
2.	Graphene-nZVI	94	162.59	172	Jabeen et al. (2011)
3.	Bentonite-nZVI	50	25	50	Shi et al. (2011)
4.	Stacked Chitosan nanofibres	n.a.	131.58	131.58	Li et al. (2015)
5.	Ionic Liquid functionalized Multiwall Carbon nanotube	n.a.	85.83	85.83	Kumar et al. (2015)
6.	Chitosan- <i>Sec</i> -Butylammonium acetate (Ionic Liquid)	n.a.	20.83	20.83	Elidordio et al. (2017)
7.	Hyperbranched polymer grafted chitosan	n.a.	194.55	194.55	Li et al. (2018)
8.	PEI-Silica nanoparticles	n.a.	183.7	183.7	Choi et al. (2018)
9.	Iminodiacetate-glycidyle methylacrylate polyethylene	n.a.	83.75	83.75	Dafader et al. (2018)
10.	Microcrystalline cellulose immobilized nZVI	12.02	52.82	490	Present study

Co(II) ions adsorption using 50–20% w/w nZVI loaded Kaolinite, an increase in the normalized adsorption of Co(II) was observed upon decreasing the nZVI loading on kaolinite. On the other hand, the interactive surface coverage area for nZVI with cellulose could not be ruled out, as cellulose plays a vital role in the regeneration of nZVI during the adsorption of Cr(VI) oxoanion. Further investigations would be required to be carried out to establish the influence of interaction surface coverage between nZVI and cellulose on the adsorption of various heavy metals.

The performance of the material CI-2 was examined by comparing the results obtained in the present study with other adsorbent normalized for the nZVI loading is depicted in Table 3. With material CI-2 obtained normalized adsorption efficiency up to 490 mg/g of nZVI for chromium, which is higher than the nZVI based adsorbents as well as the polymer functionalized material.

Conclusion

The materials CI-1-3 synthesized using ionic liquid–water binary mixture showed better water and air

stability. The effect of iron loading and the application of these materials on the chromium adsorption were investigated. The material CI-2 containing 12% w/w iron showed highest removal efficiency than CI-3 (24% w/w) and almost equal efficiency as CI-1. This is accounted to the loading behavior of iron on the cellulose surface and reaction mechanism involving iron regenerate by in situ oxidation of cellulose. The CI-I (6% w/w) and CI-2 found to have suitably spread on the cellulose with the formation of spherically shaped nZVI. In case of CI-3, higher amount of iron lead to formation of micron size particles by aggregation of nZVI particles, which decreased the adsorption efficiency of the material for chromium. The experimental data were best fitted to Langmuir and Freundlich adsorption isotherm. The adsorption process reached the adsorption equilibrium at 11 h, and the data followed pseudo second order kinetic model.

Acknowledgments Archana Kumari Sharma is thankful to CUPB for providing university fellowship for carrying out the proposed research. We are all thankful to CSMCRI, CIL-CUPB for the analytical services provided. J. N. Babu is thankful to CUPB for research seed money grant and to DST, New Delhi, India for providing funds through DST Fast Track Young Scientist as Project Ref. No. 240/2010 for research support. The authors' acknowledge Electron Microscope Division, AIIMS, New Delhi for TEM facility.

References

- Alidokht L, Khataee AR, Reyhanitabar A, Oustan S (2011) Reductive removal of Cr(VI) by starch-stabilized Fe⁰ nanoparticles in aqueous solution. *Desalination* 270:105–110
- Anirudhan TS, Jalajamony S, Suchithra PS (2009) Improved performance of a cellulose-based anion exchanger with tertiary amine functionality for the adsorption of chromium(VI) from aqueous solutions. *Colloids Surf A* 335:107–113
- APHA (2005) Standard methods for the examination of water and wastewater, 21st ed. American Public Health Association, Washington, DC, pp 3-67–3-68
- Bezbaruah AN, Krajanganpan S, Chisholm BJ, Khan E, Bermudez JJE (2009) Entrapment of iron nanoparticles in calcium alginate beads for ground water remediation application. *J Hazard Mater* 166:1339–1343
- Cai J, Kimura S, Wada M, Kuga S (2008) Nanoporous cellulose as metal nanoparticles support. *Biomacromol* 10:87–94
- Choi K, Lee S, Park JO, Park JA, Cho SH, Lee SY, Lee JH, Choi JW (2018) Chromium removal from aqueous solution by a PEI-silica nanocomposite. *Sci Rep* 8:1438
- Crane RA, Scott TB (2012) Nanoscale zero-valent iron: future prospects for an emerging water treatment technology. *J Hazard Mater* 211:112–125
- Crowhurst L, Mawdsley PR, Perez JM (2003) Solvent-solute interaction in ionic liquid. *Phys Chem Chem Phys* 5:2790–2794
- Dafader NC, Rahman N, Majumdar SK, Khan MM, Rahman MM (2018) Preparation and characterization of iminodiacetate group containing nonwoven polyethylene fabrics and its application in chromium adsorption. *J Polym Environ* 26:740–748
- Dalla Vecchia E, Coisson M, Appino C, Vinai F, Sethi R (2009) Magnetic characterization and interaction modeling of zerovalent iron nanoparticles for the remediation of contaminated aquifers. *J Nanosci Nanotechnol* 9:3210–3218
- Datta KKR, Petala E, Datta KJ, Perman JA, Tucek J, Bartak P, Zboril R (2014) NZVI modified magnetic filter paper with high redox and catalytic activities for advanced water treatment technologies. *Chem Commun* 50:15673–15676
- de Moraes Teixeira E, Corrêa AC, Manzoli A, de Lima Leite F, de Oliveira CR, Mattoso LHC (2010) Cellulose nanofibers from white and naturally colored cotton fibers. *Cellulose* 17(3):595–606
- Devan RS, Ho WD, Chen CH, Shiu HW, Ho CH, Cheng CL, Wu SY, Liou Y, Ma YR (2009) High room-temperature photoluminescence of one-dimensional Ta₂O₅ nanorod arrays. *Nanotechnology* 20:445708
- Devan RS, Lin JH, Ho WD, Wu SY, Liou Y, Ma YR (2010) Investigation of high-temperature phase transformation in one-dimensional Ta₂O₅ nanorods. *J Appl Crystallogr* 43:1062–1067
- Devan RS, Lin CL, Gao SY, Cheng CL, Liou Y, Ma YR (2011) Enhancement of green-light photoluminescence of Ta₂O₅ nanoblock stacks. *Phys Chem Chem Phys* 13:13441–13446
- Devan RS, Ma YR, More MA, Khare RT, Antad VV, Patil RA, Thakare VP, Dhayal RS, Schmidt-Mende L (2016) Promising field electron emission performance of vertically aligned one dimensional (1D) brookite (β) TiO₂ nanorods. *RSC Adv* 6:98722–98729
- Devan RS, Thakare VP, Antad VV, Chikate PR, Khare RT, More MA, Dhayal RS, Patil SI, Ma YR, Schmidt-Mende L (2017) Nano-heteroarchitectures of two-dimensional MoS₂@ one-dimensional brookite TiO₂ nanorods: prominent electron emitters for displays. *ACS Omega* 2:2925–2934
- Duan J, He X, Zhang L (2015) Magnetic cellulose–TiO₂ nanocomposite microspheres for highly selective enrichment of phosphopeptides. *Chem Commun* 51:338–341
- Eliodorio KP, Andolfatto VS, Martins MR, de Sá BP, Umeki ER, de Araújo Morandim-Giannetti A (2017) Treatment of chromium effluent by adsorption on chitosan activated with ionic liquids. *Cellulose* 24:2559–2570
- Fitz-Patrick M, Champagne P, Cunningham MF, Whitney RA (2010) A biorefinery processing perspective: treatment of lignocellulosic materials for the production of value-added products. *Bioresour Technol* 101:8915–8922
- Fu F, Wang Q (2011) Removal of heavy metal ions from wastewaters: a review. *J Environ Manag* 92:407–418
- Fu F, Ma J, Xie L, Tang B, Han W, Lin S (2013) Chromium removal using resin supported nanoscale zero-valent iron. *J Environ Manag* 128:822–827
- Fu R, Yang Y, Xu Z, Zhang X, Guo X, Bi D (2015) The removal of chromium(VI) and lead(II) from groundwater using sepiolite-supported nanoscale zero-valent iron (S-NZVI). *Chemosphere* 138:726–734
- Galan B, Castañeda D, Ortiz I (2005) Removal and recovery of Cr(VI) from polluted ground waters: a comparative study of ion-exchange technologies. *Water Res* 39:4317–4324
- Gelesky MA, Scheeren CW, Foppa L, Pavan FA, Dias SL, Dupont J (2009) Metal nanoparticle/ionic liquid/cellulose: new catalytically active membrane materials for hydrogenation reactions. *Biomacromol* 10:1888–1893
- Geng B, Jin Z, Li T, Qi X (2009) Kinetics of hexavalent chromium removal from water by chitosan-Fe⁰ nanoparticles. *Chemosphere* 75:825–830
- Gheju M (2011) Hexavalent chromium reduction with zero-valent iron (ZVI) in aquatic system. *Water Air Soil Pollut* 222:103–148
- Golder AK, Samanta AN, Ray S (2007) Removal of trivalent chromium by electrocoagulation. *Sep Purif Technol* 53:33–41
- Guo ZR, Zhang G, Fang J, Dou X (2006) Enhanced chromium recovery from tanning wastewater. *J Clean Prod* 14:75–79
- Gurgel LVA, de Melo JCP, de Lena JC, Gil LF (2009) Adsorption of chromium(VI) ion from aqueous solution by succinylated-mercerized cellulose functionalized with quaternary ammonium groups. *Bioresour Technol* 100:3214–3220
- Hafez A, El-Mariharawy S (2004) Design and performance of the two-stage/two-pass RO membrane system for chromium removal from tannery wastewater. *Desalination* 165:141–151
- Halada GP, Clayton CR (1991) Photoreduction of hexavalent chromium during X-ray photoelectron spectroscopy analysis of electrochemical and thermal films. *J Electrochem Soc* 138:2921–2927

- Harvey AE Jr, Smart JA, Amis ES (1955) Simultaneous spectrophotometric determination of iron(II) and total iron with 1,10-phenanthroline. *Anal Chem* 27:26–29
- He F, Zhao D, Liu J, Roberts CB (2007) Stabilization of Fe–Pd nanoparticles with sodium carboxymethyl cellulose for enhanced transport and dechlorination of trichloroethylene in soil and groundwater. *Ind Eng Chem Res* 46:29–34
- Hines JH, Wanigasekara E, Rudkevich DM, Rogers RD (2008) Calix[4]arenes immobilized in a cellulose-based platform for entrapment and detection of NO_x gases. *J Mater Chem* 18:4050–4055
- Horzum N, Demir MM, Nairat M, Shahwan T (2013) Chitosan fiber-supported zero-valent iron nanoparticles as a novel sorbent for sequestration of inorganic arsenic. *RSC Adv* 3:7828–7837
- Hu XJ, Wang JS, Liua YG, Li X, Zenga GM, Bao ZL, Zeng XX, Chen AW, Long F (2011) Adsorption of chromium(VI) by ethylenediamine-modified cross-linked magnetic chitosan resin: isotherms, kinetics and thermodynamics. *J Hazard Mater* 185:306–314
- Jabeen H, Chandra V, Jung S, Lee JW, Kim KS, Kim SB (2011) Enhanced Cr(VI) removal using iron nanoparticle decorated graphene. *Nanoscale* 3:3583–3585
- Jones F, Farrow JB, Van Bronswijk W (1998) An infrared study of a polyacrylate flocculant adsorbed on hematite. *Langmuir* 14:6512–6517
- Kim UJ, Kuga S (2001) Thermal decomposition of dialdehyde cellulose and its nitrogen-containing derivatives. *Thermochim Acta* 369:79–85
- Kim UJ, Wada M, Kuga S (2004) Solubilization of dialdehyde cellulose by hot water. *Carbohydr Polym* 56:7–10
- Kim JH, Kim JH, Bokare V, Kim EJ, Chang YY, Chang YS (2012) Enhanced removal of chromate from aqueous solution by sequential adsorption-reduction on mesoporous iron–iron oxide nanocomposite. *J Nanopart Res* 14:1010
- Klein-Marcuschamer D, Simmons BA, Blanch HW (2011) Techno-economic analysis of a lignocellulosic ethanol biorefinery with ionic liquid pre-treatment. *Biofuels Bioprod Biorefin* 5:562–569
- Kotelnikova N, Vainio U, Pirkkalainen K, Serimaa R (2007) Novel approaches to metallization of cellulose by reduction of cellulose-incorporated copper and nickel ions. *Macromol Symp* 254:74–79
- Koujalagi PS, Divekar SV, Kulkarni RM, Nagarale RK (2013) Kinetics, thermodynamic, and adsorption studies on removal of chromium(VI) using Tulsion A-27(MP) resin. *Desalin Water Treat* 51:3273–3283
- Kumar AS, Jiang SJ, Tseng WL (2015) Effective adsorption of chromium(VI)/Cr(III) from aqueous solution using ionic liquid functionalized multiwalled carbon nanotubes as a super sorbent. *J Mater Chem A* 3:7044–7057
- Kwak HW, Kim MK, Lee JY, Yun H, Kim MH, Park YH, Lee KH (2015) Preparation of bead-type biosorbent from water-soluble *Spirulina platensis* extracts for chromium(VI) removal. *Algal Res* 7:92–99
- Li XQ, Zhang WX (2007) Sequestration of metal cations with zerovalent iron nanoparticles a study with high resolution X-ray photoelectron spectroscopy (HR-XPS). *J Phys Chem C* 111:6939–6946
- Li XQ, Cao J, Zhang WX (2008) Stoichiometry of Cr(VI) immobilization using nanoscale zerovalent iron (nZVI): a study with high-resolution X-ray photoelectron spectroscopy (HR-XPS). *Ind Eng Chem Res* 47:2131–2139
- Li L, Li Y, Cao L, Yang C (2015) Enhanced chromium(VI) adsorption using nanosized chitosan fibers tailored by electrospinning. *Carbohydr Polym* 125:206–213
- Li Q, Xu B, Zhuang L, Xu X, Wang G, Zhang X, Chen J, Tang Y (2018) Preparation, characterization, adsorption kinetics and thermodynamics of chitosan adsorbent grafted with a hyperbranched polymer designed for Cr(VI) removal. *Cellulose* 25:3471–3486
- Liu Z, Wang H, Liu C, Jiang Y, Yu G, Mu X, Wang X (2012) Magnetic cellulose–chitosan hydrogels prepared from ionic liquids as reusable adsorbent for removal of heavy metal ions. *Chem Commun* 48:7350–7352
- Liu X, Zhou W, Qian X, Shen J, An X (2013) Polyaniline/cellulose fiber composite prepared using persulfate as oxidant for Cr(VI)-detoxification. *Carbohydr Polym* 92:659–661
- Lu P, Hsieh YL (2010) Preparation and properties of cellulose nanocrystals: rods, spheres, and network. *Carbohydr Polym* 82:329–336
- Manning BA, Kiser JR, Kwon H, Kanel SR (2007) Spectroscopic investigation of Cr(III)- and Cr(VI)-treated nanoscale zerovalent iron. *Environ Sci Technol* 41:586–592
- Matuana LM, Balatinecz JJ, Sodhi RNS, Park CB (2001) Surface characterization of esterified cellulose fibers by XPS and FTIR spectroscopy. *Wood Sci Technol* 35:191–201
- Miao Q, Yan J (2013) Comparison of three ornamental plants for phytoextraction potential of chromium removal from tannery sludge. *J Mater Cycles Waste Manag* 15:98–105
- Moulder J (1992) Handbook of X-ray photoelectron spectroscopy: a reference book of standard spectra for identification and interpretation of XPS data. Chastain J, King RC (eds) Eden Prairie, Physical Electronics Division, Perkin-Elmer Corporation, Minnesota
- Mukherjee R, Kumar R, Sinha A, Lama Y, Saha AK (2015) A review on synthesis, characterization and applications of nano-zero valent iron (nZVI) for environmental remediation. *Crit Rev Environ Sci Technol* 46:443–466
- Narayani M, Vidya SK (2012) Chromium-resistant bacteria and their environmental condition for hexavalent chromium removal: a review. *Crit Rev Environ Sci Technol* 43:955–1009
- National Toxicology Program, Department of Health and Human Services (NIEHS) (2011) Report on Carcinogens, 12th ed. <http://ntp.niehs.nih.gov/ntp/roc/twelfth/roc12.pdf>
- Owlad M, Aroua MK, Daud WAW, Baroutian S (2009) Removal of hexavalent chromium-contaminated water and wastewater: a review. *Water Air Soil Pollut* 200:59–77
- Parlayici S, Pehlivan E (2015) Natural biosorbents (garlic stem and horse chesnut shell) for removal of chromium(VI) from aqueous solutions. *Environ Monit Assess* 187:763
- Patterson JW, Passino R (1987) Metals separation and recovery. In: Patterson JW (ed) Metal speciation separation and recovery. Lewis, USA, pp 63–96
- Perez-González A, Urriaga AM, Ibáñez R, Ortiz I (2012) State of the art and review on the treatment technologies of water reverse osmosis concentrates. *Water Res* 46:267–283
- Ponder SM, Darab JG, Mallouk TE (2000) Remediation of Cr(VI) and Pb(II) aqueous solutions using supported nanoscale zerovalent iron. *Environ Sci Technol* 34:2564–2569

- Powell RM, Plus RW, Hightower SK, Sabatini DA (1995) Coupled iron corrosion and chromate reduction: mechanisms for subsurface remediation. *Environ Sci Technol* 29:1913–1922
- Qiu B, Xu C, Sun D, Wang Q, Gu H, Zhang X, Weeks BL, Hopper J, Ho T, Guo Z, Wei S (2015) Polyaniline coating with various substrates for hexavalent chromium removal. *Appl Surf Sci* 334:7–14
- Raychoudhury T, Tufenkji N, Ghoshal S (2012) Aggregation and deposition kinetics of carboxymethyl cellulose-modified zero-valent iron nanoparticles in porous media. *Water Res* 46:1735–1744
- Sajana TK, Ghangrekar MM, Mitra A (2014) Effect of presence of cellulose in the freshwater sediment on the performance of sediment microbial fuel cell. *Bioresour Technol* 155:84–90
- Saliba R, Gauthier H, Gauthier R, Petit-Ramel M (2000) Adsorption of copper(II) and chromium(III) ions onto amidoximated cellulose. *J Appl Polym Sci* 75:1624–1631
- Seid KA, Badot JC, Dubrunfaut O, Levasseur S, Guyomard D, Lestriez B (2012) Influence of the carboxymethyl cellulose binder on the multiscale electronic transport in carbon–LiFePO₄ nanocomposites. *J Mater Chem* 22:24057–24066
- Sharma YC, Srivastava V, Weng CH, Upadhyay SN (2009) Removal of Cr(VI) from wastewater by adsorption on iron nanoparticles. *Can J Chem Eng* 87:921–929
- Sharma P, Bihari V, Agarwal SK, Verma V, Kesavachandran CN, Pangtey BS, Mathur N, Singh PK, Shrivastava M, Goel SK (2012) Groundwater contaminated with hexavalent chromium [Cr(VI)]: a health survey and clinical examination of community inhabitants (Kanpur, India). *PLoS ONE* 7:e47877
- Sharma AK, Kumar R, Mittal S, Hussain S, Arora M, Sharma RC, Babu JN (2015) In-situ reductive regeneration of zerovalent iron nanoparticles immobilized on cellulose for atom efficient Cr(VI) adsorption. *RSC Adv* 5:89441–89446
- Shi LN, Zhang X, Chen ZL (2011) Removal of chromium(VI) from wastewater using bentonite-supported nanoscale zero-valent iron. *Water Res* 45:886–892
- Singh R, Misra V, Singh RP (2011) Synthesis, characterization and role of zero-valent iron nanoparticle in removal of hexavalent chromium from chromium-spiked soil. *J Nanopart Res* 13:4063–4073
- Singha AS, Guleria A (2014) Use of low cost cellulosic biopolymer based adsorbent for the removal of toxic metal ions from the aqueous solution. *Sep Sci Technol* 49:2557–2567
- Stefaniuk M, Oleszczuk P, Ok YS (2016) Review on nanozerovalent iron (nZVI): from synthesis to environmental applications. *Chem Eng J* 287:618–632
- Swatloski RP, Spear SK, Holbery JD, Rogers RD (2002) Dissolution of cellulose with ionic liquids. *J Am Chem Soc* 124:4974–4975
- Trujillo-Reyes J, Peralta-Videa JR, Gardea-Torresdey JL (2014) Supported and unsupported nanomaterials for water and soil remediation: Are they a useful solution for worldwide pollution? *J Hazard Mater* 280:487–503
- USEPA (2011) <http://www.rpi.edu/dept/chem-eng/Biotech-Environ/Adsorb/bet.htm>. Accessed 06/01/2018
- USEPA (2013) <http://www.rpi.edu/dept/chem-eng/Biotech-Environ/Adsorb/bet.htm>. Accessed 06/01/2018
- Uzum C, Shahwan T, Eroğlu AE, Hallam KR, Scott TB, Lieberwirth I (2009) Synthesis and characterization of kaolinite-supported zero-valent iron nanoparticles and their application for the removal of aqueous Cu²⁺ and Co²⁺ ions. *Appl Clay Sci* 43:172–181
- Vaid U, Mittal S, Babu JN (2013) Removal of hexavalent chromium from aqueous solution using biomass derived fly ash from waste-to-energy power plant. *Desalin Water Treat* 52:7845–7855
- Wen Z, Zhang Y, Dai C (2014) Removal of phosphate from aqueous solution using nanoscale zerovalent iron (nZVI). *Colloids Surf A Physicochem Eng Asp* 457:433–440
- Xiao S, Shen M, Guo R, Wang S, Shi X (2009) Immobilization of zerovalent iron nanoparticles into electrospun polymer nanofibers: synthesis, characterization, and potential environmental applications. *J Phys Chem C* 113:18062–18068
- Xie P, Hao X, Mohamad OA, Liang J, Wei G (2013) Comparative study of chromium biosorption by mesorhizobium-mamorrae strain CCNWS0123 in single and binary mixtures. *Appl Biochem Biotechnol* 169:570–587
- Yadav R, Sharma AK, Babu JN (2016) Sorptive removal of arsenite [As(III)] and arsenate [As(V)] by fuller's earth immobilized nanoscale zero-valent iron nanoparticles (F-nZVI): effect of Fe⁰ loading on adsorption activity. *J Environ Chem Eng* 4:681–694
- Yu X, Tong S, Ge M, Zuo J, Cao C, Song W (2013) One-step synthesis of magnetic composites of cellulose@ iron oxide nanoparticles for arsenic removal. *J Mater Chem A* 1:959–965
- Zhang Y, Xu L, Zhao L, Peng J, Li C, Li J, Zhai M (2012) Radiation synthesis and Cr(VI) removal of cellulose microsphere adsorbent. *Carbohydr Polym* 88:931–938
- Zhu S, Wu Y, Chen Q, Yu Z, Wang C, Jin S, Ding Y, Wu G (2006) Dissolution of cellulose with ionic liquids and its application: a mini-review. *Green Chem* 8:325–327